Int. J. Electrochem. Sci., 17 **(2022)** Article Number: 221263, doi: 10.20964/2022.12.71

International Journal of
ELECTROCHEMICAL
SCIENCE
www.electrochemsci.org

Preparation of Molecular Imprinted Electrochemical Sensor for Detection of Trimethylamine Oxide (TMAO) in Intestinal Flora

Xiaohui Wang[*], *Jinhua Tan, Hui Shao, Qi Cheng, Fei Kou, Bude Su, Xiaoling Yang*

Bayinguoleng Mongolian Autonomous Prefecture People's Hospital, No.41. People's East Road, Korla, Xinjiang Uygur Autonomous Region 841000 China.
[*]E-mail: ty_wxh@163.com

Received: 24 September 2022 / *Accepted:* 21 November 2022 / *Published:* 27 December 2022

Intestinal flora metabolites are the metabolites of flora microorganisms that live symbiotically with humans and are present in large numbers in the human intestine. In recent years, trimethylamine oxide (TMAO), a product related to human intestinal metabolism, has gradually attracted the attention of medical researchers, and many studies have confirmed the relevance of this substance to human cardiovascular disease, chronic kidney disease, diabetes, cancer, etc. The existing methods for the determination of TMAO include Reynolds colorimetric method, picric acid colorimetric method and ion chromatography, but these testing methods have problems such as low sensitivity, high cost, and inapplicability, which cannot meet the practical needs. Therefore, a molecularly imprinted electrochemical sensor was prepared for TMAO detection in this work. The imprinted polymer-modified electrode exhibited high recognition ability for TMAO compared to the non-imprinted polymer carbon paste electrode. The sensor was also successfully used for the sensing of TMAO in urine and swage.

Keywords: Molecular imprinting technology; Carbon nanotubes; Electrochemical sensors; Trimethylamine oxide; Template molecules

1. INTRODUCTION

In recent years, intestinal flora has developed into a research hotspot in many fields such as life sciences, food nutrition, healthcare and microbiology. Changes in gut microbes are directly related to the development of many diseases in the human body, such as cardiovascular diseases, metabolic disorders, chronic kidney diseases, and neurological disorders [1–3]. Clinical studies have shown that elevated levels of trimethylamine oxide (TMAO), a metabolite associated with intestinal flora, are associated with the risk of diabetes or different forms of atherosclerosis, including coronary artery disease (CAD) and peripheral vascular disease [4,5]. By reducing TMAO levels in germ-free mice, a significant reduction in atherosclerosis in mice was observed. TMAO has many important biological properties and has important physiological and biochemical functions such as stabilization of protein

structure, osmoregulation, resistance to ionic instability, and resistance to water stress [6]. The concentration range of TMAO in human plasma is from 0.73 to 126 μM [7,8].

The intestinal flora is an important metabolic organ in mammals and influences the overall metabolism of the host. In recent years, we have been researching to improve the means of measuring intestinal metabolites. For example, Nugent et al.[9] evaluated the metabolome of 15 colorectal adenomas and 15 normal rectal mucosal biopsies from non-adenoma controls using liquid chromatography. The abundance of specific bacterial taxa was measured by real-time fluorescence quantitative PCR, and a total of 274 metabolites were identified for studying the relationship between intestinal entry metabolites and colorectal adenomas. Further studies by Zheng et al.[10] found that melamine can be produced in the intestinal tract by microbial transformation of melamine, which can cause kidney damage. This is a component of the kidney stones that contribute to melamine-induced nephrotoxicity in rats. This further suggests that the toxicity of melamine may depend on the exact composition and metabolic activity of the intestinal flora. Therefore, the accurate determination of intestinal flora metabolites is of great significance in the study of disease mechanisms and prevention and control of mutual intestinal flora and host metabolism. It is now hypothesized that the main role of *Echinococcus granulosus* infection in reducing inflammatory damage in the colon is the immunomodulatory effect of the Echinococcus cystic fluid antigen AgB, a major component of the cyst fluid [11,12]. It inhibits the polarization of macrophages toward M1-type, decreases Th1-type cytokine expression, and increases Th2-type cytokine expression. At the same time, fine grain *Echinococcus granulosus* infection and AgB alter the local immune and flora characteristics of the intestine, thus protecting the colon from inflammatory injury [13]. The intestinal flora also interacts in the natural and acquired immune systems in the state of parasitic infection. Changes in the immune status of infection can promote the colonization of the corresponding microorganisms in the gut, and the microbial community can integrate into the physiological system of the body and influence the dynamic balance of the body through the immune system [14,15].

Molecular imprinting technology (MIT) is a branch of discipline that has been developed in recent years by combining the advantages of many disciplines such as polymer synthesis, molecular design, molecular recognition, and bionanotechnology [16,17]. In recent years, MIT has penetrated into areas including drug analysis, environmental monitoring, and food safety. The MIT is essentially very similar to the principle of antigen-antibody, enzyme-substrate specific binding. It is the process of selecting a target molecule as a template and preparing a polymer that has specific selection and recognition functions for the template molecule [18]. In the preparation of molecularly imprinted polymers, the first step is the formation of a prepolymer from a specific template molecule and its matching functional monomer through covalent and non-covalent bonding (hydrogen bonding, electrostatic gravity, metal chelation, charge transfer, hydrophobic interaction, and van der Waals forces) [19]. The second step is to add the appropriate amount of crosslinker and initiator and polymerize under suitable conditions, and finally the prepolymer is fixed in a three-dimensional mesh structure. The third step is to remove the template molecule from the structure by physical and chemical methods. This leaves binding sites in the structure that match the spatial configuration of the template molecule [20].

In this work, we constructed a novel electrochemical sensor for the detection of TMAO based on MIT and photopolymerization techniques. The electrochemical behavior of TMAO on bare carbon paste

electrodes (CPE), MIP/CPE, carbon nanotube-modified carbon paste electrodes (MIP/MWCNTs/CPE), and NIP/MWCNTs/CPE was investigated. The results show that MIP/MWCNTs/CPE have higher sensitivity and selectivity compared with other electrodes.

2. EXPERIMENTAL

2.1. Chemicals and instruments

TMAO, potassium chloride and potassium ferricyanide [$K_3Fe(CN)_6$] were purchased from Lingyike Chemical Co. Acrylic acid (AA), azo diisobutyronitrile (AIBN) were purchased from Meike Chemical Co. Ethylene glycol dimethyl acrylate (EGDMA) was purchased from Shanghai Jingpu Reagent Co. Multi-walled carbon nanotubes (MWCNT) were purchased from Shenzhen Nanoport Co. Phosphate buffer solution (PBS) was prepared with K_2HPO_4 and KH_2PO_4 in ultrapure water. All other reagents were analytically grade.

Electrochemical data were obtained from a CHI832 electrochemical workstation (CHI, Shanghai C&H Instruments, Inc.). A three-electrode system was used for chemical measurements: the reference electrode was a silver/silver chloride electrode (Ag/AgCl) and a platinum wire electrode was used as counter electrode. CPE, MWCNTs modified electrodes (MIP/MWCNTs/CPE, NIP/MWCNTs/CPE) were used as working electrodes. TMAO detection was carried out using a 0.1 M pH=7.0 PBS as the supporting electrolyte. The differential pulse voltammogram (DPV) is recorded by scanning between 0 ~ 0.8 V with a pulse amplitude of 50 mV. EIS was tested by scanning in 5 mM $K_3[Fe(CN)_6]$ and 0.1 M KCl solution.

2.2. Preparation of molecularly imprinted polymers

Molecularly imprinted polymers are prepared by photopolymerization. In this process, TMAO is the template molecule, AA is the functional monomer, EGDMA is the crosslinker, and AIBN is the initiator. The template molecule TMAO (2 mM), equal amounts of AA (molar ratio between template molecule and functional monomer: 1:1, 1:2, 1:4, 1:6) and 20 mL of dichloromethane were put into a 50 mL round bottom flask, mixed well and left for 2 h. Subsequently, 24 mM EGDMA and 0.5 mM AIBN were added, mixed thoroughly, and placed in a refrigerator (4°C) for 12 h, followed by 2 h of photopolymerization in an ice bath. Finally, the template molecules were eluted by placing the polymer powder in H_2SO_4 (0.1 M) solution with sufficient stirring for 3 h. The preparation of the non-imprinted polymer is the same as above except that TMAO is not added during the polymerization process.

2.3. Preparation of sensors

Concentrated HNO_3 and MWCNT were mixed in the ratio of 100:1 (mL/g), and the multi-walled carbon nanotube solution was centrifuged after ultrasonic shaking for 1 h. MWCNT was washed with secondary distilled water to neutral and dried in an oven. Accurately weigh 12 mg of graphite powder

with 6 mg of the prepared molecularly imprinted polymer powder into an agate mortar. Then, 0.20 mL of paraffin oil and 3 mg of MWCNT were added and well ground. Finally, the resulting carbon paste is pressed firmly and polished to make the surface of the electrode smooth. The preparation of bare carbon paste electrodes is similar to that of MIP/MWCNTs/CPE, except that molecularly imprinted polymer powder is not added to the mixture.

3. RESULTS AND DISCUSSION

Figure 1 shows the FTIR spectra of TMAO removed-MIP, MIP and NIP. It can be seen from the figure that the absorption peak at 1719.42 cm^{-1} indicates the stretching vibration of C=O The absorption peaks of MIP at 1388.51 cm^{-1}, 1150.74 cm^{-1}, 1638.21 cm^{-1} represent the stretching vibration of S=O [21]. The template molecule TMAO was removed by elution, which made the above peaks almost disappeared, and the absorption spectrum of its spectrum was almost identical to that of NIP, indicating that the template molecule was completely removed. Meanwhile, the above conclusion also indicates that the molecular imprinting complex can be formed between AA and TMAO by hydrogen bonding [22].

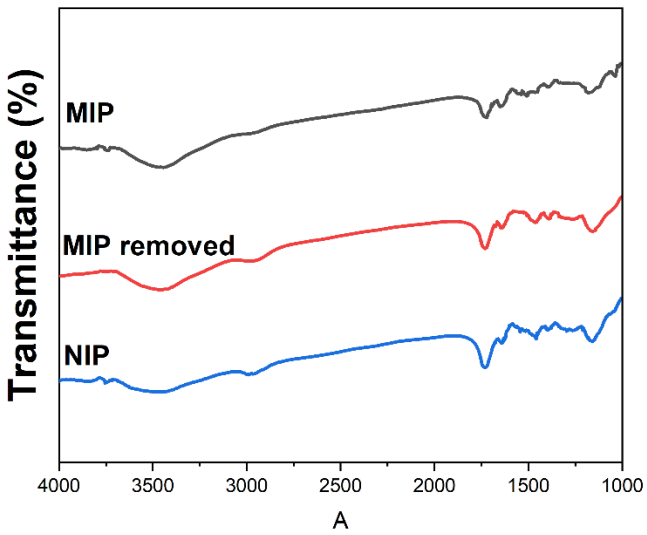

Figure 1. FTIR spectra of TMAO removed-MIP, MIP and NIP.

Figure 2 shows the DPV response of the different modified electrodes in PBS (pH=7.0) solution. As can be seen, NIP/CPE and NIP/MWCNTs/CPE are almost a straight line, indicating that the electrode has almost no electrochemical response to TMAO. When the carbon paste was doped with molecularly imprinted polymer, the oxidation peak of TMAO appeared at 0.73 V, indicating that the imprinted electrode has some specific recognition performance for TMAO [23]. When MWCNT was further doped, the peak current increased by more than 10 times, indicating that the high specific surface area and excellent electronic conductivity of MWCNT promoted the electrochemical response of TMAO on the electrode surface [24]. Moreover, the oxidation peak current of TMAO was significantly increased

on MIP/MWCNTs/CPE compared with that on bare electrode. Therefore, the electrochemical response to TMAO with MIP/MWCNTs/CPE is better compared with other modified electrodes.

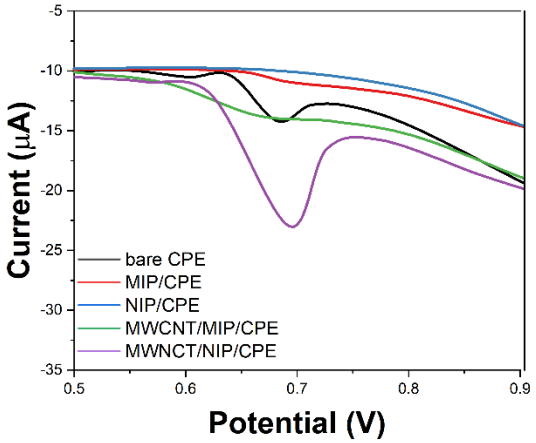

Figure 2. DPVs of NIP/CPE, MIP/CPE, bare CPE, NIP/MWCNTs/CPE and MIP/MWCNTs/CPE toward 1 μM TMAO in pH=7.0 PBS.

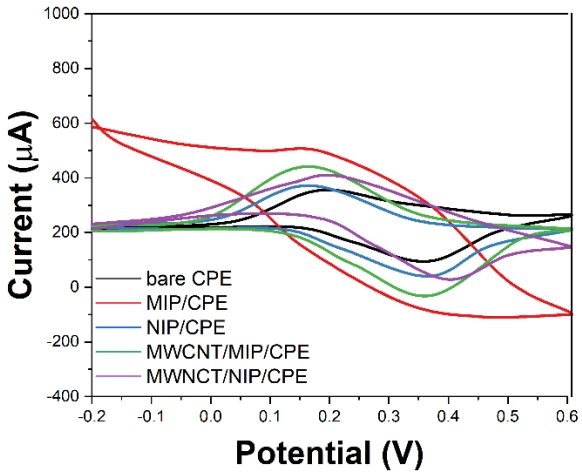

Figure 3. CV of 1 mM $Fe(CN)_6^{3-/4-}$ and 0.1 M KCl at MIP/MWCNTs/CPE, MIP/MWCNTs/CPE removed, MWCNTs/CPE, bare CPE and NIP/MWCNTs/CPE. Scan rate: 50 mV/s.

We have characterized the various prepared electrodes with different modifications using $[Fe(CN)_6]^{3-}$/$[Fe(CN)_6]^{4-}$ as the probe and 0.1 M HCl using CV and EIS, respectively (Figure 3). A pair of distinct redox peaks of $K_3[Fe(CN)_6]$ was observed on the bare CPE. The peak currents were significantly increased after the modification of MWCNT, which was attributed to the increase of the specific surface area of the electrode by MWCNT [25]. The redox peak current of $[Fe(CN)_6]^{3-}$ before the removal of the template by MIP/MWCNTs/CPE was reduced due to the doping of the carbon paste with molecularly imprinted polymers. Part of the surface of the electrode is occupied by MIP, which hinders the electron transfer [26]. The peak current increases when the template is removed from MIP/MWCNTs/CPE due to the generation of holes on the electrode surface after the template molecules

are eluted. This hole allows the smooth transfer of the $[Fe(CN)_6]^{3-/4-}$ ion pair to the electrode surface. The redox peak current of $[Fe(CN)_6]^{3-/4-}$ at NIP/MWCNTs/CPE is significantly lower due to the doping of the carbon paste with non-molecularly imprinted polymers [27]. Part of the electrode surface is occupied by NIP, which is non-conductive and thus hinders the electron transfer.

EIS is an effective method to further investigate the interfacial properties of different modified electrodes. Figure 4A shows Nyquist plots of different electrodes. The impedance values (Rct) for CPE and MWCNTs/CPE were 58.4 Ω and 47.2 Ω, respectively. On MWCNTs/CPE, the impedance curve is almost a straight line because the mass diffusion limits the electron transfer process and indicates a faster electron transfer rate [28]. A comparison of the two shows that MWCNTs/CPE have a significant facilitation effect and lower electron transfer resistance, while for MIP/MWCNTs/CPE, the resistance value is significantly higher (Figure 4B). The impedance values (Rct) of MIP/MWCNTs/CPE, NIP/MWCNTs/CPE and MIP/MWCNTs/CPE after removing the template are 471.1 Ω, 485.7 Ω and 197.2 Ω, respectively. From the results of the fitted impedance values, it is clear that for NIP/MWCNTs/CPE, the lack of TMAO molecules at the time of polymer formation and the poor conductivity of the polymer film hinder the transfer of $[Fe(CN)_6]^{3-/4-}$ ion pairs [29]. However, when the template molecules are removed, the carbon paste modified electrode surface generates many cavities, which allow the $[Fe(CN)_6]^{3-/4-}$ ion pairs to pass to the electrode surface [30]. Therefore, the capacitive component plays a very significant role in modifying the current of the electrode.

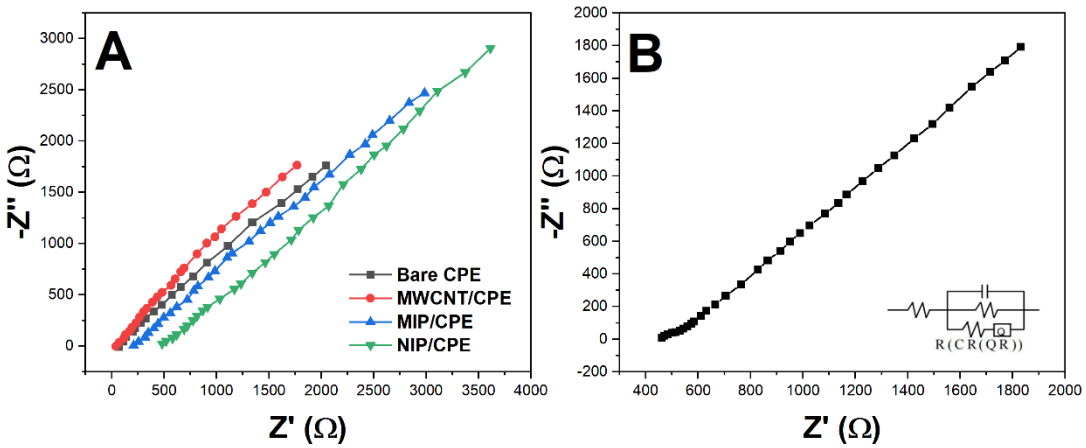

Figure 4. (A) EIS plots and (B) simulated equivalent circuit diagram of different electrodes in 5 mM $K_3[Fe(CN)_6]$.

We investigated the different ratios between template molecules and functional monomers (Figure 5). The results show that the peak current value is maximum when the ratio of the two reaches 1:2. When the ratio continues to increase, the peak current decreases continuously. This is related to the change in the specific surface area of the electrode and the electron transfer resistance [31]. When the ratio between TMAO and AA is too large, the interaction force between TMAO and AA becomes weak and easy to be destroyed [32]. Very few of the cavities on the surface of molecularly imprinted polymer

films are occupied by TMAO, and their peak currents are reduced. In contrast, when the ratio between the two is too small, there are fewer recognition sites for AA to interact with the template molecule and the peak current decreases.

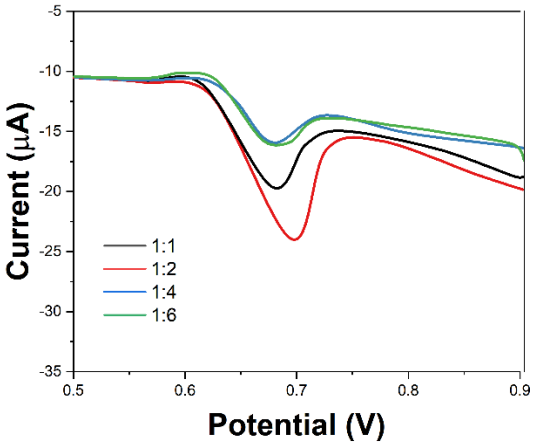

Figure 5. The influence of ratio between TMAO and AA (1:1 to 1:6) of MIP/MWCNTs/CPE towards determination of 1 μM TMAO.

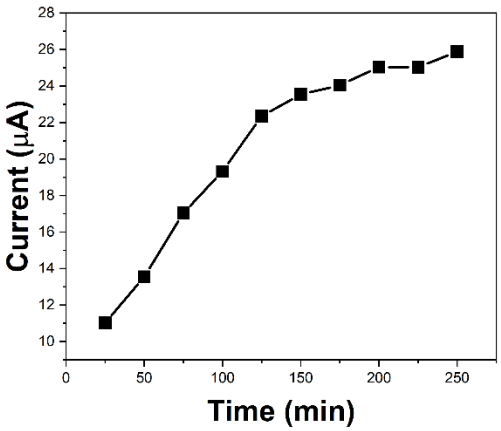

Figure 6. The influence of elution time of MIP/MWCNTs/CPE towards determination of 1 μM TMAO.

The elution time can affect the current response. To determine the optimal elution time for use in the TMAO assay, we recorded the DPV response of the blotted polymers at different elution times in PBS (0.2 M, pH=7.0) solution containing 0.1 M KCl (Figure 6). The DPV response of TMAO is decreasing with increasing elution time. When the time reaches 200 min, the peak current almost disappears. This indicates that the template molecules have been eluted by 200 min. Therefore, we adopted 200 min as the optimal elution time in the subsequent experiments.

Solution pH is one of the very important parameters in practical applications. We investigated the electrochemical response of TMAO in various buffer solutions (pH range 4 ~ 9) (Figure 7A). The anodic peak current increases with increasing pH and then decreases when the pH reaches 7.0 (Figure 7B). The relationship between the pH value of the solution and the anodic peak potential (Ep) of TMAO was also investigated. With increasing pH, its oxidation peak potential gradually shifts in a negative direction, which suggests the involvement of protons in the electrochemical reaction of TMAO [33]. The corresponding trend of oxidation potential (Epa) versus pH obeys the functional equation (Figure 7C): Epa(V) = -0.032pH + 0.9333. According to the Nernst equation, the number of electrons transferred in the electrochemical reaction is twice as many as the number of protons transferred [34]. The oxidation of TMAO is a deprotonation process, and each molecule produces one proton and one electron during the oxidation process.

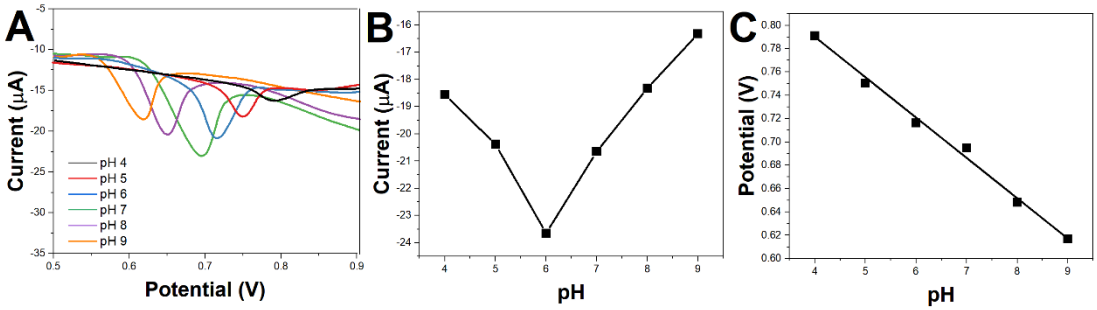

Figure 7. (A) DPV of MIP/MWCNTs/CPE in 0.2 M PBS at different pHs. (B) Plot of peak current vs. pH values. (C) Plots of E vs. pH.

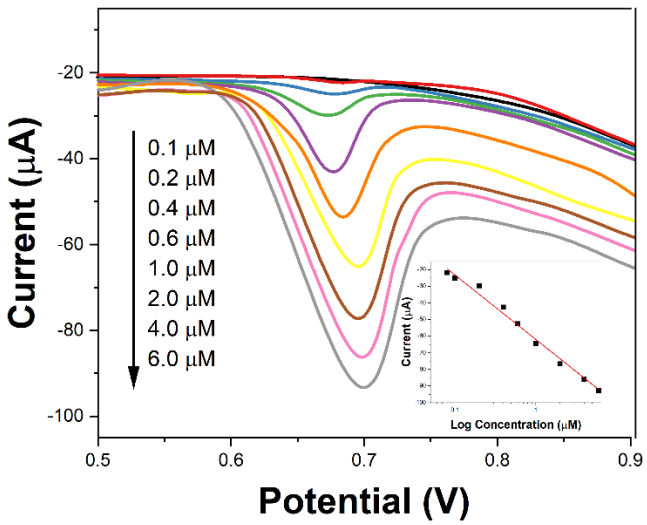

Figure 8. DPVs of TMAO concentration(from a to i): 80 nM, 0.1 μM, 0.2 μM, 0.4 μM, 0.6 μM, 1 μM, 2 μM, 4 μM, 6 μM at MIP/MWCNTs/ CPE. Insets: The calibration curves of related concentrations.

To obtain the linear dynamic range of the modified electrode for the detection of TMAO under optimal conditions, we investigated the DPV response of the analyte TMAO in phosphate buffer at pH=7.0 (Figure 8). It can be seen that the oxidation peak current of TMAO increases with increasing concentration at MIP/MWCNTs/CPE. Its concentration showed a good linearity with peak current in the range of 0.08-6 μM. The detection limit was 26 nM (S/N=3).

To examine the selectivity of the molecularly imprinted sensor for TMAO, we added 100-fold inorganic ions Ca^{2+}, Cu^{2+}, Cl^{-}, NO_3^{-} and 20-fold glucose and ascorbic acid under the same experimental conditions. The results demonstrated that none of these interference species had any effect on the detection of TMAO (Figure 9), indicating that the sensor has a high selectivity for TMAO. In addition, this indicates that the unique shape of the template molecule plays a very important role in the selective binding to the polymer.

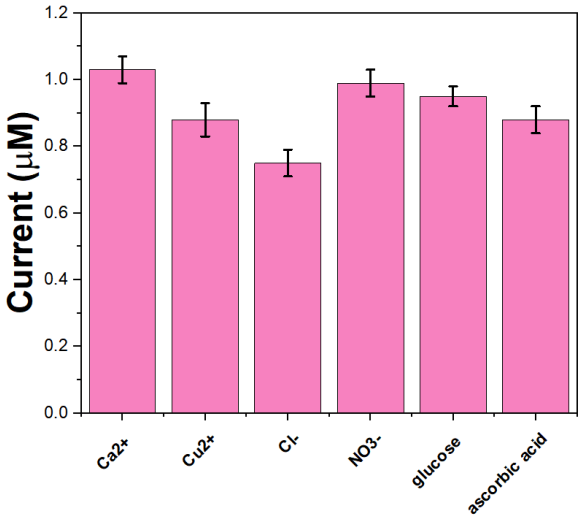

Figure 9. Influence of coexistent substance on the electrochemical response of MIP/MWCNTs/CPE to TMAO.

The practical applicability of the MIP/MWCNTs/CPE assay can be further investigated by measuring the TMAO content in real samples. Human urine samples and sewage were selected as the actual samples for analysis. The assay was performed under experimental optimal conditions. Among them, each group of actual samples was measured three times in parallel, and the results are shown in Table 1. The results demonstrate that the proposed electrochemical sensor can be applied to the TMAO detection in real samples.

Table 1. TMAO results from human urine and sewage.

Sample	Found (μM)	Added (μM)	Detection (μM)	Recovery (%)	RSD (%)
Urine 1	1.22	2.00	3.27	101.55	3.33
Urine 2	1.41	2.00	3.38	99.12	3.21
Swage 1	-	2.00	1.97	98.50	2.50
Swage 2	-	2.00	1.96	98.00	3.12

4. CONCLUSION

In this work, we constructed a fast, simple and inexpensive molecularly imprinted polymer-modified carbon paste electrode. The proposed electrode was successfully used for the detection of TMAO in real samples. Due to the advantages of multi-walled carbon nanotubes and molecularly imprinted polymers, the sensor showed high sensitivity and good selectivity for the detection of TMAO. The oxidation process of TMAO involves a proton and an electron. Under optimal conditions, the concentration of TMAO showed a good linear relationship with its peak current in the range of 0.08-6 μM, with a detection limit of 26 nM.

ACKNOWLEDGEMENTS
This work has been financially supported by State Key Laboratory of Pathogenesis, Prevention and Treatment of Central Asian High Incidence Diseases Fund and Science and Technology Research Plan of Bayingolin Mongolian Autonomous Prefecture

References

1. R. Jalandra, N. Dalal, A.K. Yadav, D. Verma, M. Sharma, R. Singh, A. Khosla, A. Kumar, P.R. Solanki, *Appl. Microbiol. Biotechnol.*, 105 (2021) 7651–7660.
2. H. Vallance, A. Koochin, J. Branov, A. Rosen-Heath, T. Bosdet, Z. Wang, S. Hazen, G. Horvath, *Mol. Genet. Metab. Rep.*, 15 (2018) 130–133.
3. G. Yang, C.-C. Lin, Y. Yang, L. Yuan, P. Wang, X. Wen, M.-H. Pan, H. Zhao, C.-T. Ho, S. Li, *J. Agric. Food Chem.*, 67 (2019) 6169–6176.
4. A.B. Bockus, B.A. Seibel, *Comp. Biochem. Physiol. A. Mol. Integr. Physiol.*, 217 (2018) 35–42.
5. H. Al-Rubaye, G. Perfetti, J.-C. Kaski, *Curr. Probl. Cardiol.*, 44 (2019) 182–196.
6. K. Jaworska, K. Bielinska, M. Gawrys-Kopczynska, M. Ufnal, *Cardiovasc. Res.*, 115 (2019) 1948–1949.
7. K. Jaworska, M. Konop, T. Hutsch, K. Perlejewski, M. Radkowski, M. Grochowska, A. Bielak-Zmijewska, G. Mosieniak, E. Sikora, M. Ufnal, *J. Gerontol. Ser. A*, 75 (2020) 1276–1283.
8. S. Lv, Y. Wang, W. Zhang, H. Shang, *Heart*, 108 (2022) 917–922.
9. J.L. Nugent, A.N. McCoy, C.J. Addamo, W. Jia, R.S. Sandler, T.O. Keku, *J. Proteome Res.*, 13 (2014) 1921–1929.
10. X. Zheng, A. Zhao, G. Xie, Y. Chi, L. Zhao, H. Li, C. Wang, Y. Bao, W. Jia, M. Luther, *Sci. Transl. Med.*, 5 (2013) 172ra22-172ra22.
11. A.D. Permana, A.J. Paredes, F.V. Zanutto, M.N. Amir, I. Ismail, M.A. Bahar, Sumarheni, S.D. Palma, R.F. Donnelly, *ACS Appl. Mater. Interfaces*, 13 (2021) 38745–38760.
12. M.M. Aljedaie, E.S. Al-Malki, *J. King Saud Univ.-Sci.*, 32 (2020) 2810–2817.
13. V. Ranaei, Z. Pilevar, C. Esfandiari, A.M. Khaneghah, R. Dhakal, E. Vargas-Bello-Pérez, H. Hosseini, *Food Sci. Anim. Resour.*, 41 (2021) 16.
14. K.P. Labrada, S. Strobl, B. Eckmair, M. Blaukopf, Z. Dutkiewicz, A. Hykollari, D. Malzl, K. Paschinger, S. Yan, I.B. Wilson, *ACS Chem. Biol.*, 15 (2020) 369–377.
15. W. Lin, J. Zhang, J.-F. Xu, J. Pi, *Front. Pharmacol.* (2021) 1971.
16. M.L. Yola, N. Atar, *Compos. Part B Eng.*, 175 (2019) 107113.
17. X. Ma, X. Tu, F. Gao, Y. Xie, X. Huang, C. Fernandez, F. Qu, G. Liu, L. Lu, Y. Yu, *Sens. Actuators B Chem.*, 309 (2020) 127815.
18. Y. Lai, Y. Deng, G. Yang, S. Li, C. Zhang, X. Liu, *J. Biomed. Nanotechnol.*, 14 (2018) 1688–1694.

19. Q. Yang, C. Li, J. Li, X. Wang, M. Arabi, H. Peng, H. Xiong, L. Chen, *Nanoscale*, 12 (2020) 6529–6536.
20. Q. Yang, J. Li, X. Wang, H. Peng, H. Xiong, L. Chen, *Biosens. Bioelectron.*, 112 (2018) 54–71.
21. Y. Liu, G. Li, Q. Han, H. Lin, Q. Li, G. Deng, F. Liu, *J. Membr. Sci.*, 641 (2022) 119900.
22. G.B.V.S. Lakshmi, A.K. Yadav, N. Mehlawat, R. Jalandra, P.R. Solanki, A. Kumar, *Sci. Rep.*, 11 (2021) 1338.
23. Y. Yi, A. Liang, L. Luo, Y. Zang, H. Zhao, A. Luo, *Bioelectrochemistry*, 144 (2022) 108038.
24. A.F. Waffo, B. Mitrova, K. Tiedemann, C. Iobbi-Nivol, S. Leimkühler, U. Wollenberger, *Biosensors*, 11 (2021) 98.
25. B. Mitrova, A.F. Waffo, P. Kaufmann, C. Iobbi-Nivol, S. Leimkühler, U. Wollenberger, *ChemElectroChem*, 6 (2019) 1732–1737.
26. Y.-C. Chang, Y.-H. Chu, C.-C. Wang, C.-H. Wang, Y.-L. Tain, H.-W. Yang, *Biosensors*, 11 (2021) 339.
27. Y. Hu, X. Han, L. Shi, B. Cao, *Electrochimica Acta* (2022) 140917.
28. E.M. Al-Khalqi, M.A. Abdul Hamid, N.H. Al-Hardan, L.K. Keng, A. Jalar, *J. Mater. Sci. Mater. Electron.*, 33 (2022) 1618–1630.
29. M. Jablonski, A. Poghossian, M. Keusgen, C. Wege, M.J. Schöning, *Anal. Bioanal. Chem.*, 413 (2021) 5669–5678.
30. A. Poghossian, M.J. Schöning, *Sensors*, 20 (2020) 5639.
31. Y. Ito, J. Okuda-Shimazaki, W. Tsugawa, N. Loew, I. Shitanda, C.-E. Lin, J. La Belle, K. Sode, *Biosens. Bioelectron.*, 129 (2019) 189–197.
32. N.E. Tolouei, S. Ghamari, M. Shavezipur, *J. Electroanal. Chem.*, 878 (2020) 114598.
33. J.M. Lim, J.H. Kim, M.Y. Ryu, C.H. Cho, T.J. Park, J.P. Park, *Anal. Chim. Acta*, 1026 (2018) 109–116.
34. E.M. Al-Khalqi, M.A. Abdul Hamid, N.H. Al-Hardan, L.K. Keng, *Sensors*, 21 (2021) 2110.